

Sunspot activity and the long-term variation of the Sun's open magnetic flux

Y.-M. Wang and N. R. Sheeley Jr.

E. O. Hulburt Center for Space Research, Naval Research Laboratory, Washington, D. C., USA

Received 4 September 2001; revised 19 October 2001; accepted 24 October 2001; published 17 October 2002.

[1] The interplanetary magnetic field (IMF) originates in open magnetic regions of the Sun (coronal holes), which in turn form mainly through the emergence and dispersal of active region fields. The radial IMF strength is proportional to the total open flux Φ_{open} , which can be estimated from source surface extrapolations of the measured photospheric field, after correction for magnetograph saturation effects. We derive the long-term variation of Φ_{open} during 1971–2000 and discuss its relation to sunspot activity. The average value of Φ_{open} was $\sim 20\text{--}30\%$ higher during 1976–1996 than during 1971–1976 and 1996–2000, with major peaks occurring in 1982 and 1991. Near sunspot minimum, most of the open flux resides in the large polar coronal holes, whereas at sunspot maximum it is rooted in relatively small, low-latitude holes located near active regions and characterized by strong footpoint fields; since the decrease in the total area occupied by holes is offset by the increase in their average field strengths, Φ_{open} remains roughly constant between activity minimum and maximum, unlike the total photospheric flux Φ_{tot} . The long-term variation of Φ_{open} approximately follows that of the Sun's total dipole strength, with a contribution from the magnetic quadrupole around sunspot maximum. Global fluctuations in sunspot activity lead to increases in the equatorial dipole strength and hence to enhancements in Φ_{open} and the IMF strength lasting typically ~ 1 year. We employ simulations to clarify the role of active region emergence and photospheric transport processes in the evolution of the open flux. Representing the initial field configuration by one or more bipolar magnetic regions (BMRs), we calculate its subsequent evolution under the influence of differential rotation, supergranular convection, and a poleward bulk flow. The initial value of Φ_{open} is determined largely by the equatorial dipole strength, which in turn depends on the longitudinal phase relations between the BMRs. As the surface flow carries the BMR flux to higher latitudes, the equatorial dipole is annihilated on a timescale of ~ 1 year by the combined effect of rotational shearing and turbulent diffusion. The remaining flux becomes concentrated around the poles, and Φ_{open} approaches a limiting value that depends on the axisymmetric dipole strengths of the original BMRs. The polar coronal holes thus represent the long-lived, axisymmetric remnant of the active regions that emerged earlier in the cycle. **INDEX TERMS:** 1650 Global Change: Solar variability; 2162 Interplanetary Physics: Solar cycle variations (7536); 7511 Solar Physics, Astrophysics, and Astronomy: Coronal holes; 7524 Solar Physics, Astrophysics, and Astronomy: Magnetic fields; **KEYWORDS:** coronal holes, interplanetary magnetic field, open flux, solar activity cycle, solar magnetic field, solar variability

Citation: Wang, Y.-M., and N. R. Sheeley Jr., Sunspot activity and the long-term variation of the Sun's open magnetic flux, *J. Geophys. Res.*, 107(A10), 1302, doi:10.1029/2001JA000500, 2002.

1. Introduction

[2] The interplanetary magnetic field (IMF) has its source in open magnetic regions of the Sun, identified observationally with coronal holes. Since the latitudinal distribution, areal sizes, polarities, and surface field strengths of coronal holes are known to undergo systematic variations over the sunspot cycle, it is not surprising that the IMF should also

show cycle-related variations. The relationship between the IMF sector structure, the topology of the heliospheric current sheet, and the evolution of the Sun's large-scale magnetic field has been explored extensively in the past [see, e.g., Svalgaard and Wilcox, 1975; Hoeksema et al., 1982]. Rather less attention has been paid to the solar cycle variations in the IMF strength, although it is increasingly recognized that such variations may have important effects at Earth [see, e.g., Lockwood and Stamper, 1999; Cane et al., 1999].

[3] Ulysses magnetometer measurements over the past decade have shown that the magnitude, $|B_r|$, of the radial

IMF component is essentially independent of heliographic latitude and longitude at heliocentric distances of order 1 AU [Balogh *et al.*, 1995; Smith *et al.*, 2001]. From flux conservation it follows that $|B_r| \sim \Phi_{\text{open}}/(4\pi r^2)$, where r denotes heliocentric radius and Φ_{open} is the total amount of open flux (both inward and outward) crossing the solar surface. This result greatly simplifies the problem of understanding the variation of the IMF strength, by reducing it to that of relating the single parameter Φ_{open} to the evolution of the photospheric magnetic field.

[4] This paper discusses the nature and causes of the long-term variation of Φ_{open} , expanding on and updating earlier studies by Wang *et al.* [2000a, 2000b]. After describing our procedure for estimating the total open flux from solar magnetograph observations, we analyze the relationship between this quantity and sunspot activity over the last 30 years. We then present simulations demonstrating how open flux is generated and destroyed through the emergence and decay of active regions.

2. Deriving the Open Flux From Photospheric Field Measurements

[5] To determine both the total open flux and its distribution over the solar surface from the observed photospheric field, we use the potential field source surface (PFSS) method. Let λ denote heliographic latitude and ϕ denote Carrington longitude (increasing westward in the direction of the solar rotation). In the PFSS model the coronal magnetic field $\mathbf{B}(r, \lambda, \phi)$ is assumed to satisfy the current-free condition $\nabla \times \mathbf{B} = 0$ out to a spherical “source surface” at $r = R_{ss} = 2.5 R_S$, where the effect of the quasi-radial solar wind outflow is simulated by requiring that $B_\lambda = B_\phi = 0$ [Schatten *et al.*, 1969]. The boundary condition at the photosphere is taken as

$$B_r(R_S, \lambda, \phi) = B_{\text{los}}(R_S, \lambda, \phi)/\cos\lambda, \quad (1)$$

where B_{los} is the observed line-of-sight component of the photospheric field; this radial matching condition takes into account the quasi-radial and nonpotential nature of the magnetic field at the depth where it is measured [Wang and Sheeley, 1992]. Solution of Laplace's equation then yields the three components of the coronal field as expansions involving the spherical harmonic functions $Y_{lm}(\lambda, \phi)$. All field lines that extend from $r = R_S$ to $r = R_{ss}$ are defined to be “open.” The magnetic field at the source surface may be expressed as

$$B_r(R_{ss}, \lambda, \phi) = \sum_{l=1}^{\infty} \sum_{m=-l}^{m=+l} c_l a_{lm} Y_{lm}(\lambda, \phi), \quad (2)$$

where

$$c_l = \frac{(2l+1)(R_S/R_{ss})^{l+2}}{l+1+l(R_S/R_{ss})^{2l+1}}, \quad (3)$$

$$a_{lm} = \int B_r(R_S, \lambda, \phi) Y_{lm}^*(\lambda, \phi) d\Omega. \quad (4)$$

In equation (4) the integral is taken over all solid angles Ω , while the asterisk denotes a complex conjugate. The total open flux is then given by

$$\phi_{\text{open}} = R_{ss}^2 \int |B_r(R_{ss}, \lambda, \phi)| d\Omega. \quad (5)$$

[6] For the photospheric field data, we employ 27.3-day Carrington maps from the Mount Wilson Observatory (MWO) and the Wilcox Solar Observatory (WSO). At both observatories the magnetograph measurements are made in the Fe I 5250 Å line. It is well known that most of the photospheric flux is concentrated in narrow, unresolved bundles having characteristic strengths of order 10^3 G [see, e.g., Zwaan, 1987]. Because the corresponding Zeeman splitting in the magnetically sensitive Fe I 5250 Å line is comparable to the line width (so that the cores of the left- and right-circularly polarized components are shifted into the sampling pass bands on each side of line center), the magnetograph intensity signal is “saturated” and the magnetic flux is underestimated. The saturation effect decreases toward the solar limb because of the falloff of the magnetic field with height. By performing simultaneous measurements in Fe I 5250 Å and Fe I 5233 Å, which saturates only at field strengths as high as ~ 4000 G, Ulrich [1992] (see also the discussion by Ulrich *et al.* [2002]) derived a correction factor for the Fe I 5250 Å fluxes as a function of center-to-limb angle. We approximate his result by means of the analytical function

$$f_{5250}(\lambda) = 4.5 - 2.5 \sin^2 \lambda \quad (6)$$

[see Wang and Sheeley, 1995]. Both the MWO and WSO data are scaled upward by this factor, which varies from 4.5 at the equator to 2 at the poles. In part because of calibration problems affecting the MWO magnetograph after it was rebuilt at the end of 1981, we will use WSO observations for the period 1976–1995 and MWO observations only during 1971–1976 and 1995–2000. We have chosen not to employ photospheric field maps from the National Solar Observatory/Kitt Peak (made in the Fe I 8688 Å line) because of their relatively uncertain zero level.

[7] As has been demonstrated in previous studies [Wang *et al.*, 1996; Neugebauer *et al.*, 1998], the PFSS model reproduces surprisingly well the observed distribution of He I 10830 Å coronal holes; it is thus likely to yield a reasonably good estimate of the total open flux Φ_{open} threading the solar surface. However, the model cannot describe the angular distribution of the open flux at heliocentric distances $r \gtrsim R_{ss}$, because it does not include the effect of the current sheet(s) generated by the interaction between the solar wind plasma and the coronal magnetic field [see, e.g., Suess *et al.*, 1977; Mikic and Linker, 1996; Wang *et al.*, 1998; Zhao and Hoeksema, 1994]. These sheet currents, located where B_r reverses its sign, act to redistribute the open flux so that it becomes asymptotically independent of λ and ϕ [see Schatten, 1971; Wolfson, 1985]. As a result, the radial field strength at $r = r_E = 1$ AU is given simply by

$$B_{\text{open}}^E = \phi_{\text{open}}/(4\pi r_E^2). \quad (7)$$

[8] The derived values of B_{open}^E during 1971–2000 are shown by the solid curve in Figure 1. Also plotted for

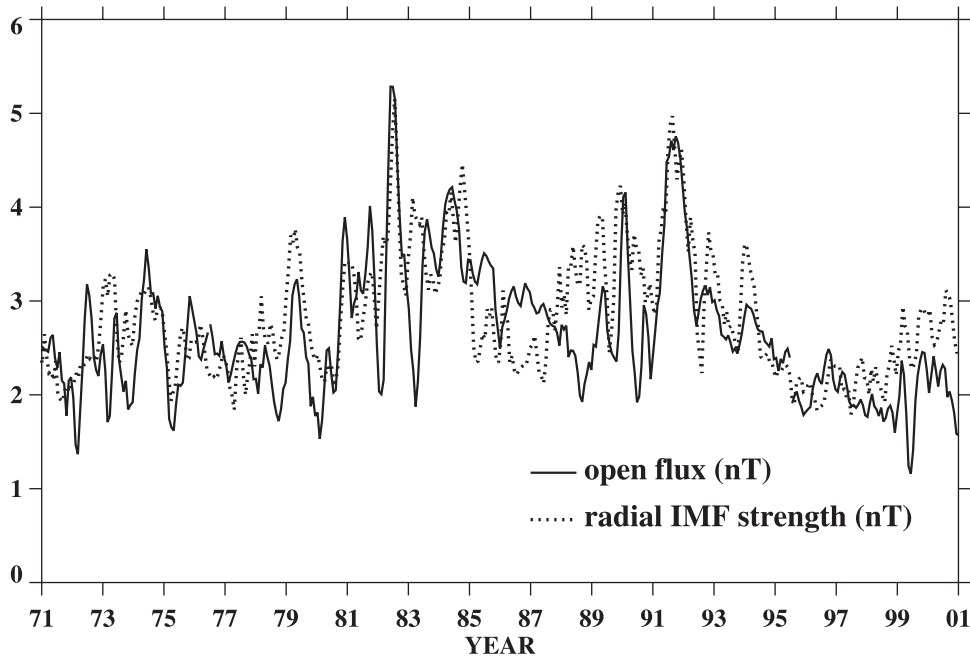


Figure 1. Long-term variation of the Sun's total open flux Φ_{open} , divided by $4\pi r_E^2$ to convert it into a field strength (nT) at 1 AU (solid curve). Also plotted for comparison is the measured near-Earth radial interplanetary magnetic field (IMF) strength $|B_x|$ (dotted curve). Here and in Figures 2, 3, 4, 5, and 7, 3-month running means have been taken. In deriving Φ_{open} a potential field source surface (PFSS) extrapolation was applied to monthly photospheric field maps from Mount Wilson Observatory (MWO) (Carrington rotations (CR) 1568–1643, 1897–1972) and Wilcox Solar Observatory (WSO) (CR 1642–1898), after correcting them for magnetograph saturation effects.

comparison are the in situ measurements of $|B_x|$, the near-Earth radial IMF strength (dotted curve). In both cases, 3-month running means are displayed, based respectively on the values of Φ_{open} computed for each Carrington rotation and on daily values of $|B_x|$ downloaded from the National Space Science Data Center (NSSDC) OMNIWeb site. Through most of the 30-year interval, B_{open}^E shows reasonably good agreement with $|B_x|$, both in its magnitude and in the shape of its fluctuations. The average strength of the derived and observed fields was $\sim 20\text{--}30\%$ higher during 1976–1996 than during 1971–1976 and 1996–2000. Especially noteworthy is the coincidence between the major peaks in B_{open}^E and $|B_x|$ in 1982 and 1991. The largest discrepancies occurred during 1986–1988, perhaps because of errors in measuring the strong polar fields at that time. The overall correlation coefficient of B_{open}^E and $|B_x|$ is 0.67, and the mean value of B_{open}^E ($|B_x|$) over the entire 30-year period was 2.6 nT (2.8 nT). We point out that the model does not include the effect of coronal mass ejections (CMEs), which may cause significant short-term fluctuations in the Sun's open flux around sunspot maximum [see, e.g., *Cliver and Ling, 2001*]. However, the rough agreement between the magnitudes of B_{open}^E and $|B_x|$ suggests that the net contribution of CMEs to the radial field strength at Earth is at most of order 20% near sunspot maximum.

3. Open Flux and Sunspot Activity, 1971–2000

[9] Having established the general correspondence between the total open flux and the observed IMF strength,

we proceed to analyze in detail the solar cycle variation of Φ_{open} .

[10] Of particular interest is the relationship between Φ_{open} and the total photospheric flux,

$$\Phi_{\text{tot}} = R_S^2 \int |B_r(R_S, \lambda, \phi)| d\Omega, \quad (8)$$

which includes both closed and open magnetic fields. Figure 2 shows the variation of Φ_{open} and Φ_{tot} during 1971–2000, with both quantities plotted on the same scale; also indicated are the monthly mean sunspot numbers R_Z (dotted curve). (In deriving Φ_{tot} we have again employed WSO data for the period 1976–1995 and MWO data for the remaining intervals. Because the magnitude of Φ_{tot} depends to some extent on the spatial resolution of the photospheric field measurements, we have scaled the MWO values downward by 20% to match those obtained from the lower-resolution WSO maps.) It is evident that Φ_{open} undergoes considerably less solar cycle modulation than Φ_{tot} ; the factors by which their amplitudes vary are ~ 2 and ~ 4 , respectively. The ratio $\Phi_{\text{tot}}/\Phi_{\text{open}}$ increases from ~ 2.5 at sunspot minimum to ~ 8 at sunspot maximum, when the photospheric field is dominated by closed flux in the form of active region loops. While fluctuations in Φ_{tot} and R_Z are generally accompanied by fluctuations in Φ_{open} , there appears to be no simple relationship between the heights of the corresponding peaks. Moreover, the solar cycle modulation of Φ_{open} (like that of $|B_x|$) lags Φ_{tot} and R_Z by 1–2 year, with its maxima occurring in 1982 and 1991, just as sunspot activity was beginning to decline. Computed for the entire interval

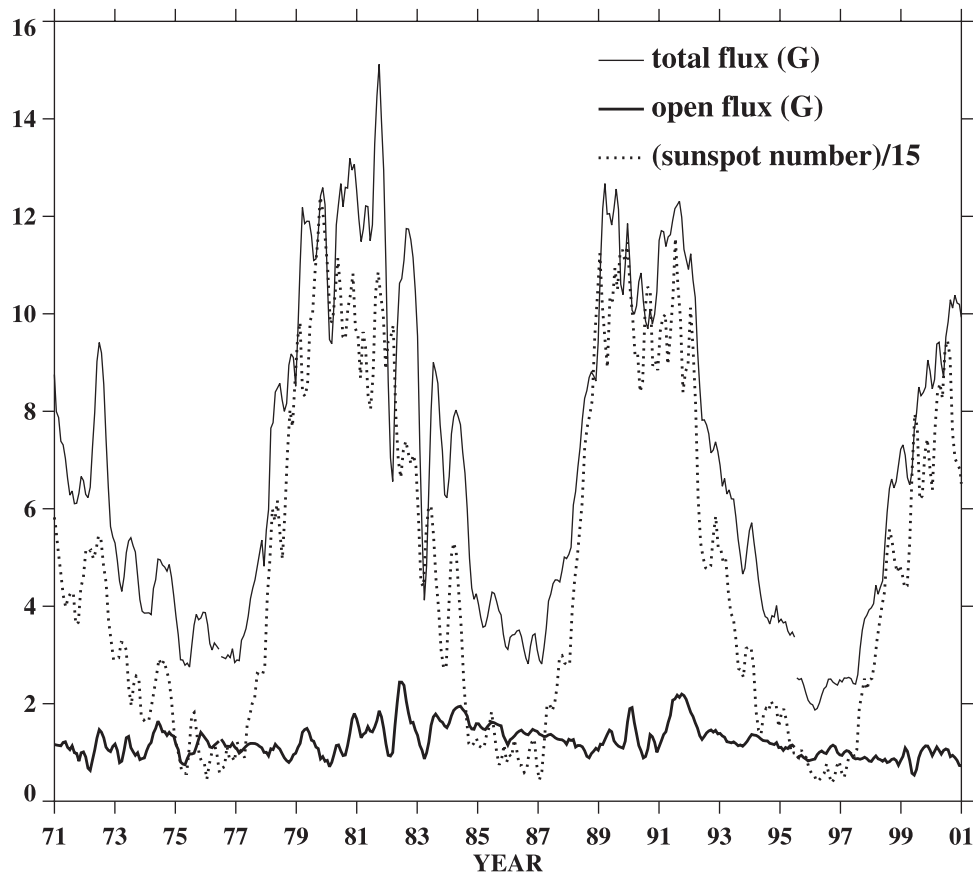


Figure 2. Variation of the total (closed and open) photospheric flux Φ_{tot} , open flux Φ_{open} , and sunspot numbers R_Z during 1971–2000 (3-month running means). Both Φ_{tot} and Φ_{open} have been divided by $4\pi R_S^2$ to convert them into equivalent field strengths (G) averaged over the solar surface. The MWO total photospheric fluxes during 1971–1976 and 1995–2000 have been multiplied by a factor of 0.8 to bring them into register with the lower-resolution WSO measurements.

1971–2000, the correlation coefficient of Φ_{open} and Φ_{tot} is 0.32 (as compared with 0.95 for the correlation between Φ_{tot} and R_Z).

[11] When averaged over time, there is a general tendency for Φ_{open} to depend on the overall activity level and amount of photospheric flux emergence during each 11-year cycle. That Φ_{open} and the radial IMF strength were, on average, ~ 20 – 30% higher during 1976–1996 than during 1971–1976 and 1996–2000 reflects the relatively large values of Φ_{tot} and R_Z during sunspot cycles 21 and 22.

[12] We now consider the properties of the footpoint regions of the open flux (“coronal holes”), which can be located by tracing magnetic field lines downward from the source surface or upward from the photosphere. Figure 3 shows the variation of A_{open} and $\langle B_{\text{open}} \rangle$ during 1971–2000, where A_{open} is the total surface area occupied by open flux and $\langle B_{\text{open}} \rangle \equiv \Phi_{\text{open}}/A_{\text{open}}$ is the average field strength within these holes. It is seen that the percentage of the Sun’s surface covered by open flux decreases from $\sim 20\%$ near sunspot minimum to $\sim 5\%$ at sunspot maximum but that $\langle B_{\text{open}} \rangle$ increases from ~ 5 G to ~ 20 G at the same time; thus the product $\langle B_{\text{open}} \rangle A_{\text{open}} = \Phi_{\text{open}}$ remains roughly the same at solar minimum and maximum. *Harvey et al.* [1982] reached a similar conclusion by comparing He I λ 10830

coronal holes with photospheric magnetograms during 1975–1980.

[13] In Figure 4 we plot separately the high-latitude ($|\lambda| > 45^\circ$) and low-latitude ($|\lambda| < 45^\circ$) contributions to Φ_{open} during 1971–2000. It is apparent that most of the open flux originates above 45° near sunspot minimum but below 45° near sunspot maximum. These high- and low-latitude sources may be identified respectively with the polar coronal holes, which extend down to an average latitude of $|\lambda| \sim 60^\circ$ near sunspot minimum, and with the smaller holes that form inside decaying active regions around sunspot maximum (see Figure 2 of *Wang et al.* [1996]). The total open flux and the IMF strength tend to peak during the early declining phase of each cycle (see Figure 1), when both the low- and high-latitude components contribute.

[14] The four curves in Figure 5 show Φ_{open} and Φ_{tot} separated into their Northern and Southern Hemisphere components. Especially striking are the large north-south asymmetries present in the open flux during the 1989–1991 activity maximum. It is evident that the Southern Hemisphere was the main source of the 1991 peak in the total open flux and IMF strength (Figure 1) and that this peak coincided with a surge of sunspot activity in the Southern Hemisphere. In general, we see a marked tendency for the

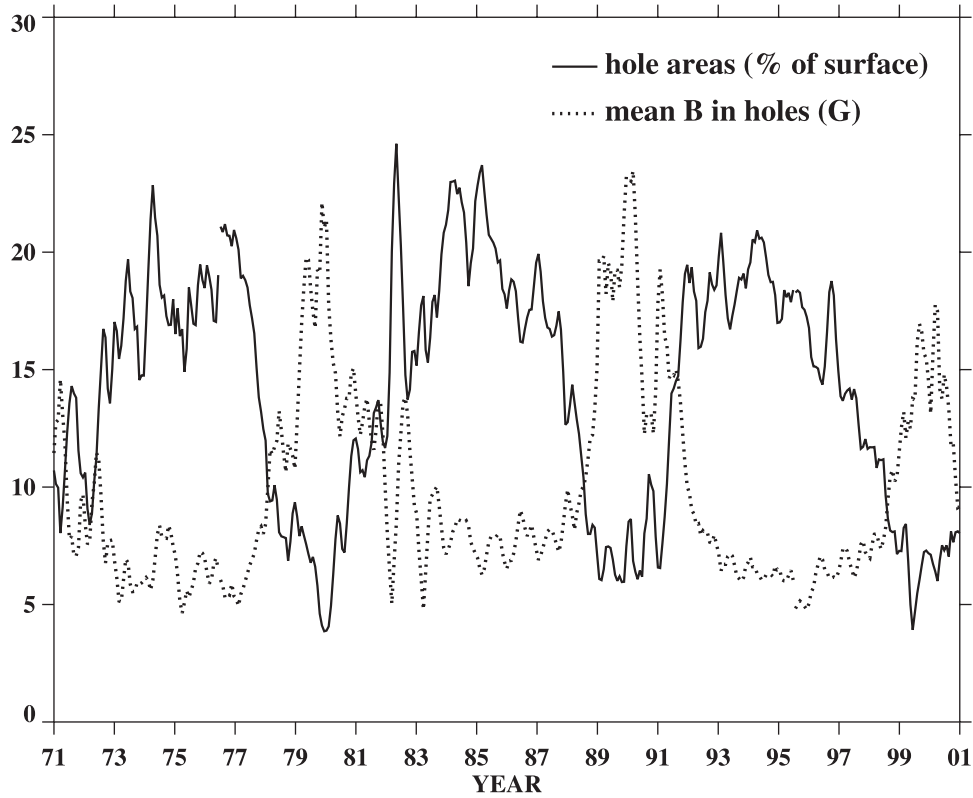


Figure 3. Time variation of the total surface area occupied by open flux, $A_{\text{open}}/(4\pi R_S^2)$ (percentage of the solar surface), and of the average field strength within open regions, $\langle B_{\text{open}} \rangle \equiv \Phi_{\text{open}}/A_{\text{open}}$ (G).

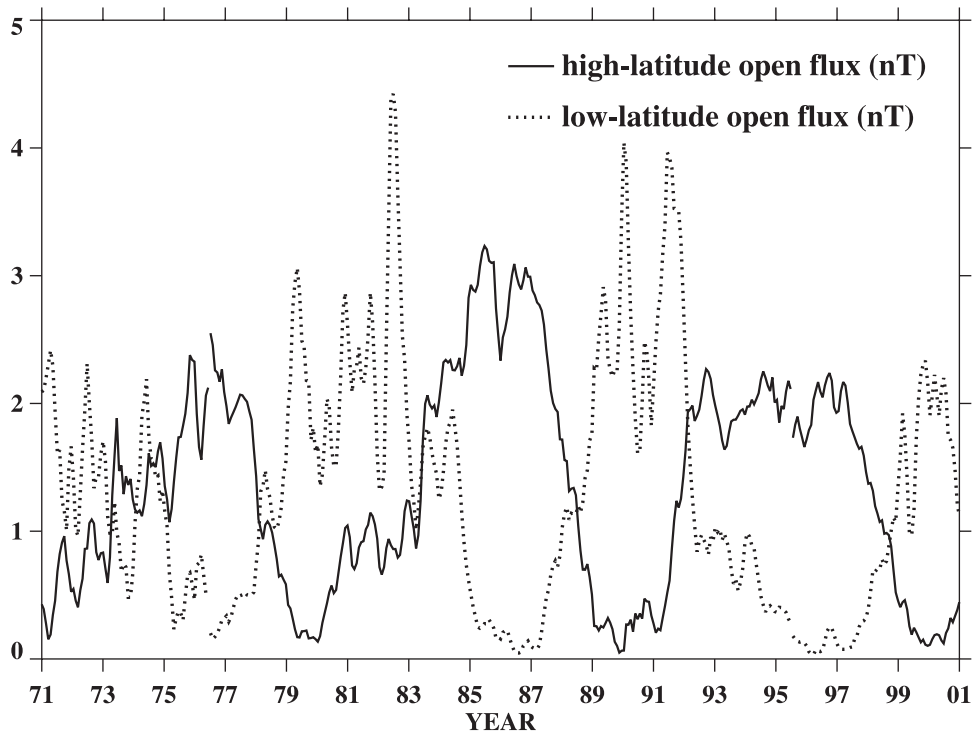


Figure 4. Time variation of the open flux originating from high latitudes, $\Phi_{\text{open}}(|\lambda| > 45^\circ)/(4\pi r_E^2)$ (nT), and from low latitudes, $\Phi_{\text{open}}(|\lambda| < 45^\circ)/(4\pi r_E^2)$ (nT).

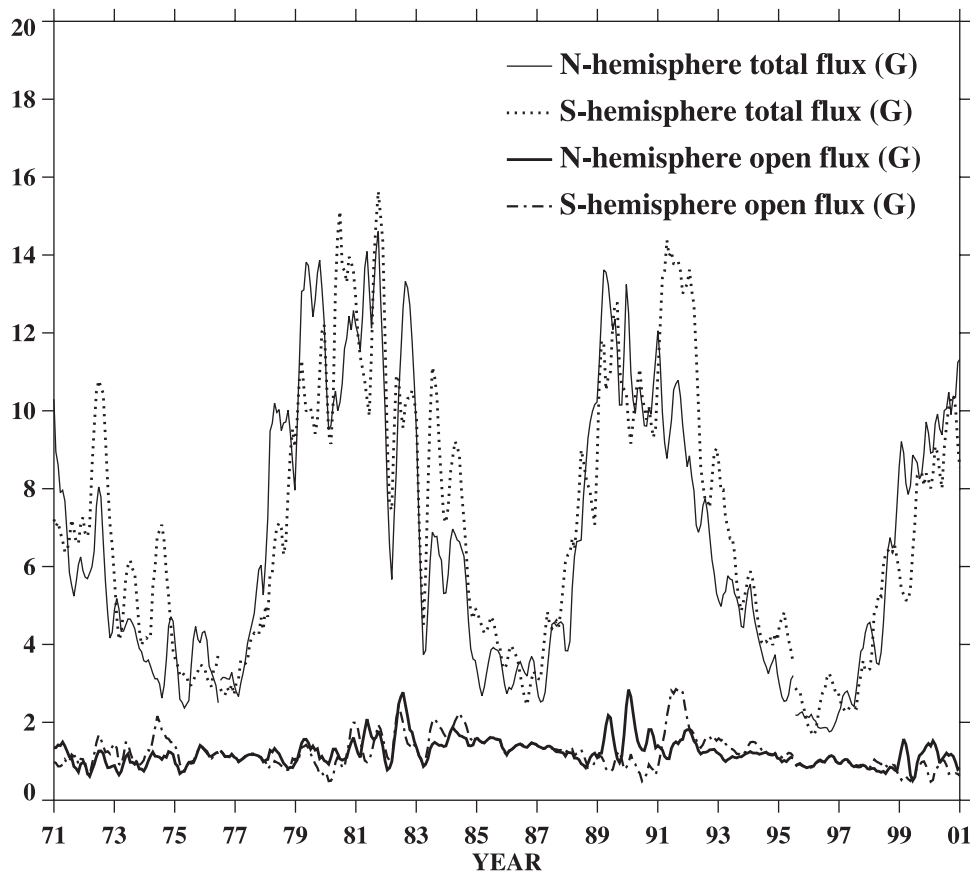


Figure 5. Time variation of the open flux originating in the Northern Hemisphere, $\Phi_{\text{open}}(\lambda > 0^\circ)/(2\pi R_S^2)$ (G), the open flux originating in the Southern Hemisphere, $\Phi_{\text{open}}(\lambda < 0^\circ)/(2\pi R_S^2)$ (G), the total photospheric flux in the Northern Hemisphere, $\Phi_{\text{tot}}(\lambda > 0^\circ)/(2\pi R_S^2)$ (G), and the total photospheric flux in the Southern Hemisphere, $\Phi_{\text{tot}}(\lambda < 0^\circ)/(2\pi R_S^2)$ (G).

Southern (Northern) Hemisphere to be more active in the declining (rising) phase of the last few solar cycles. However, this particular pattern did not persist through earlier cycles, as demonstrated by *White and Trotter* [1977], who plotted the variation of sunspot areas in each hemisphere during 1874–1971 and concluded that the north-south asymmetries were randomly distributed over this longer interval.

[15] In Figure 6 we display latitude-time plots (“butterfly diagrams”) of open flux $\langle |B_{\text{open}}| \rangle_\phi \cos \lambda$, total flux $\langle |B_r| \rangle_\phi \cos \lambda$, and net flux $\langle B_r \rangle_\phi \cos \lambda$ at the photosphere. All of the magnetic fluxes are binned in uniform latitude intervals at the solar surface and averaged over longitude. The low-latitude open flux tends to be “clumpy,” with the bigger clumps (which are often asymmetrically distributed between the Northern and Southern Hemispheres) showing faint poleward extensions directed forward in time. The largest such concentration occurs in 1991 in the Southern Hemisphere, in a region where the total photospheric flux is also strongly enhanced. Comparing the maps of open and net photospheric flux, we see that the faint wings emanating from the clumps correspond to trailing-polarity fields surging from the sunspot latitudes toward the poles. (The role of these meridional-flow-driven surges in canceling and regenerating the polar fields is discussed by *Howard and LaBonte* [1981] and *Wang et al.* [1989a]; compare also the flux

transport simulations below.) It is also seen that the vanishing of the high-latitude open flux during 1971, 1979–1980, 1989–1991, and 1999–2000 coincides with the times of polar field reversal, whereas the disappearance of the low-latitude open flux around sunspot minimum reflects the decreased rate of flux emergence and the migration of the net photospheric flux to the polar regions.

4. Open Flux and the Lowest-Order Multipoles of the Photospheric Field

[16] Further insight into the variation of the open flux can be obtained by considering its multipole constituents. As indicated by equation (2), the source surface field $B_{ss} \equiv B_r(R_{ss}, \lambda, \phi)$ can be expressed as a sum over all multipoles l , in which each term is multiplied by the coefficient $c_l \propto (R_{ss}/R_S)^{-l-2}$. Because of the rapid falloff of c_l with l , only the lowest-order multipoles contribute significantly to B_{ss} and hence to $\Phi_{\text{open}} = R_{ss}^2 \int |B_{ss}| d\Omega$. To measure the average strength of a given multipole or spherical harmonic component at the source surface, we rewrite equation (2) in the general form

$$B_{ss} = \sum_{l=1}^{\infty} b_l(\lambda, \phi) = \sum_{l=1}^{\infty} \sum_{m=0}^{m=l} b_{lm}(\lambda, \phi), \quad (9)$$

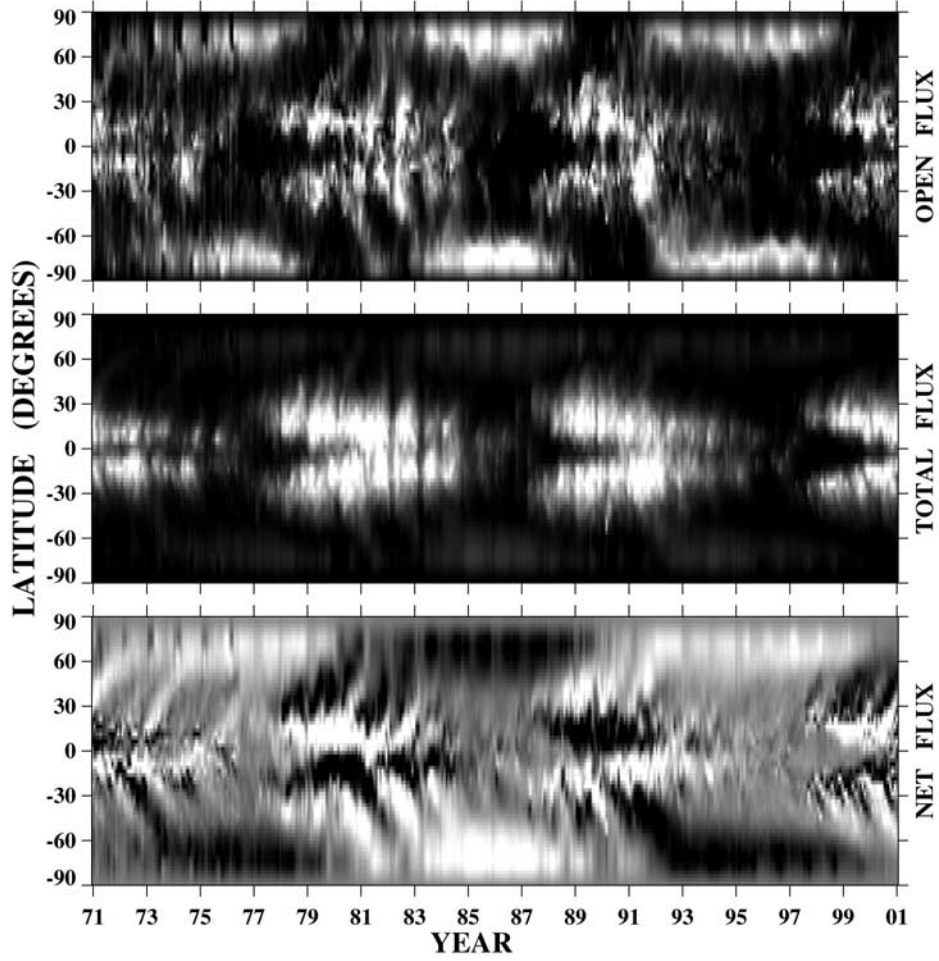


Figure 6. Latitude-time distribution of (from top to bottom) open, total, and net photospheric flux. The magnetic fluxes are binned in equal latitude intervals at the photosphere and averaged over longitude. In the top panel, white (black) denotes $\langle |B_{\text{open}}| \rangle_{\phi} \cos \lambda > 3$ G ($\langle |B_{\text{open}}| \rangle_{\phi} \cos \lambda = 0$ G). In the middle panel, white (black) denotes $\langle |B_r| \rangle_{\phi} \cos \lambda > 18$ G ($\langle |B_r| \rangle_{\phi} \cos \lambda < 1$ G). In the bottom panel, white (black) denotes $\langle B_r \rangle_{\phi} \cos \lambda > +3$ G ($\langle B_r \rangle_{\phi} \cos \lambda < -3$ G). The annual modulation seen in the high-latitude fluxes is an artifact caused by the Sun's 7.25° axial tilt.

and define

$$\langle b_l \rangle \equiv \int |b_l(\lambda, \phi)| d\Omega / 4\pi, \quad (10)$$

$$\langle b_{lm} \rangle \equiv \int |b_{lm}(\lambda, \phi)| d\Omega / 4\pi. \quad (11)$$

Of particular significance are the dipole strengths, which take the explicit form

$$\langle b_1 \rangle = (c_1/4\pi) \int |v \sin \lambda + h_1 \cos \lambda \cos \phi + h_2 \cos \lambda \sin \phi| d\Omega, \quad (12)$$

$$\langle b_{10} \rangle = (c_1/4\pi) \int |v \sin \lambda| d\Omega, \quad (13)$$

$$\langle b_{11} \rangle = (c_1/4\pi) \int |h_1 \cos \lambda \cos \phi + h_2 \cos \lambda \sin \phi| d\Omega. \quad (14)$$

Here, $c_1 = 0.093$ and

$$v = (3/4\pi) \int B_r(R_S, \lambda, \phi) \sin \lambda d\Omega, \quad (15)$$

$$h_1 = (3/4\pi) \int B_r(R_S, \lambda, \phi) \cos \lambda \cos \phi d\Omega, \quad (16)$$

$$h_2 = (3/4\pi) \int B_r(R_S, \lambda, \phi) \cos \lambda \sin \phi d\Omega. \quad (17)$$

[17] Figure 7a compares the long-term variations of $\langle b_1 \rangle$, $\langle b_2 \rangle$, and Φ_{open} . Through most of the interval 1971–2000, Φ_{open} closely tracks the total dipole strength $\langle b_1 \rangle$ (with a correlation of 0.90). The quadrupole component $\langle b_2 \rangle$ contributes significantly to the total open flux only around sunspot maximum.

[18] Figure 7b shows the relationship between Φ_{open} and the equatorial (nonaxisymmetric) dipole strength $\langle b_{11} \rangle$; also

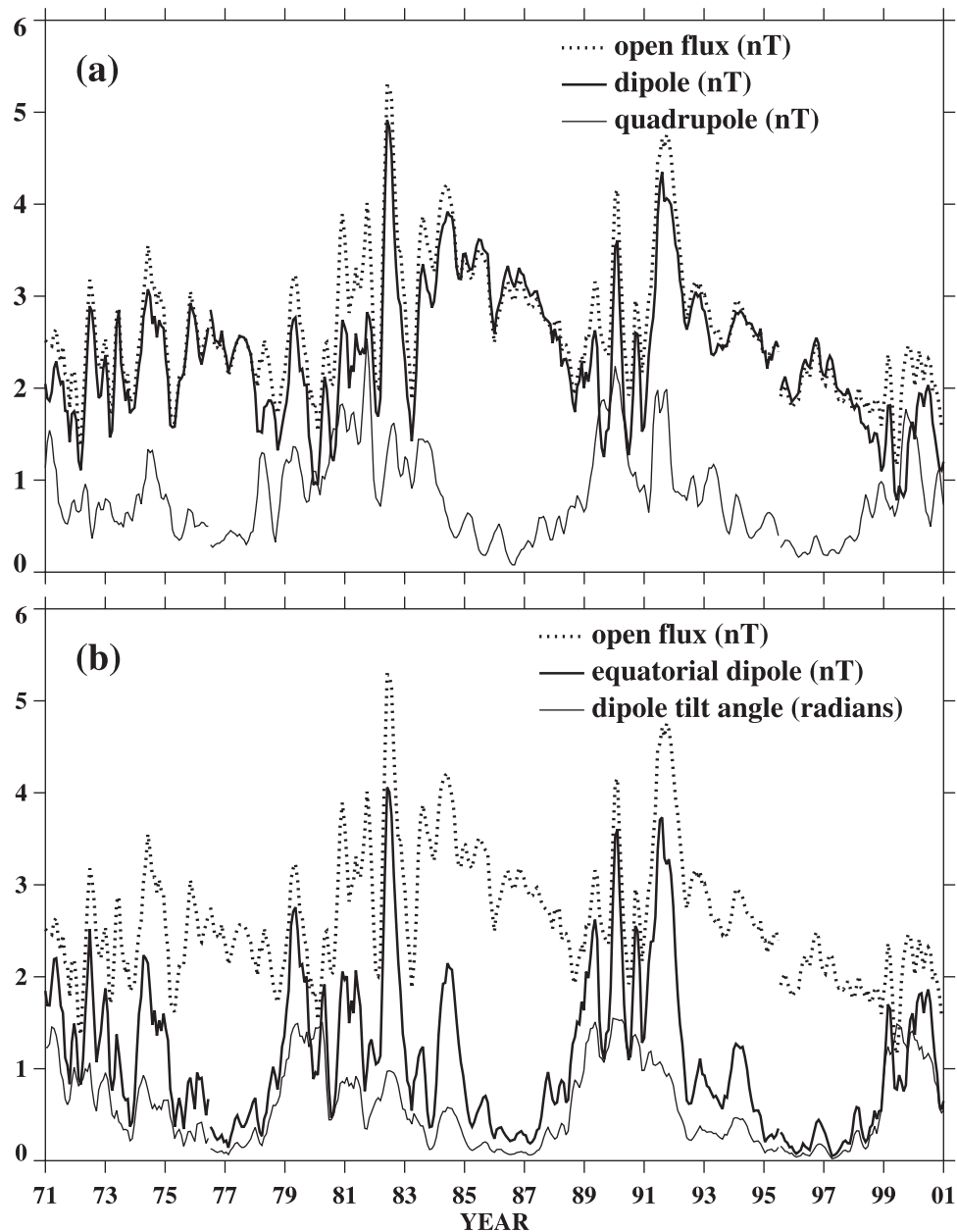


Figure 7. (a) Time variation of $\langle b_1 \rangle (R_{ss}/r_E)^2$, $\langle b_2 \rangle (R_{ss}/r_E)^2$, and $\Phi_{\text{open}}/(4\pi r_E^2)$ (all in nT). (b) Time variation of $\langle b_{11} \rangle (R_{ss}/r_E)^2$ and $\Phi_{\text{open}}/(4\pi r_E^2)$ (nT); also plotted is the dipole tilt angle δ , measured in radians relative to the nearest pole.

plotted is the dipole tilt angle δ (i.e., the angle between the dipole and rotation axes), defined by

$$\cos \delta = |v|/(v^2 + h_1^2 + h_2^2)^{1/2}. \quad (18)$$

It is apparent that the fluctuations in Φ_{open} on timescales of ~ 1 year correspond to large enhancements in $\langle b_{11} \rangle$. The equatorial dipole field has its main source in the sunspot latitudes, as a comparison between the variation of $\langle b_{11} \rangle$ and that of the low-latitude open flux (Figure 4) suggests. The oscillatory behavior of $\langle b_{11} \rangle$ reflects the spatially and temporally nonuniform nature of sunspot activity, in which flux emerges in large active region complexes that grow and

decay on timescales of a few months to more than a year [see *Gaizauskas et al.*, 1983].

5. Generation and Decay of Open Flux: The Flux Transport Model

[19] We now discuss the physical mechanisms underlying the long-term evolution of the open flux. Employing numerical simulations, we demonstrate how Φ_{open} is determined by the emergence of active region fields and by their subsequent dispersal over the solar surface by differential rotation, supergranular convection, and meridional bulk flow.

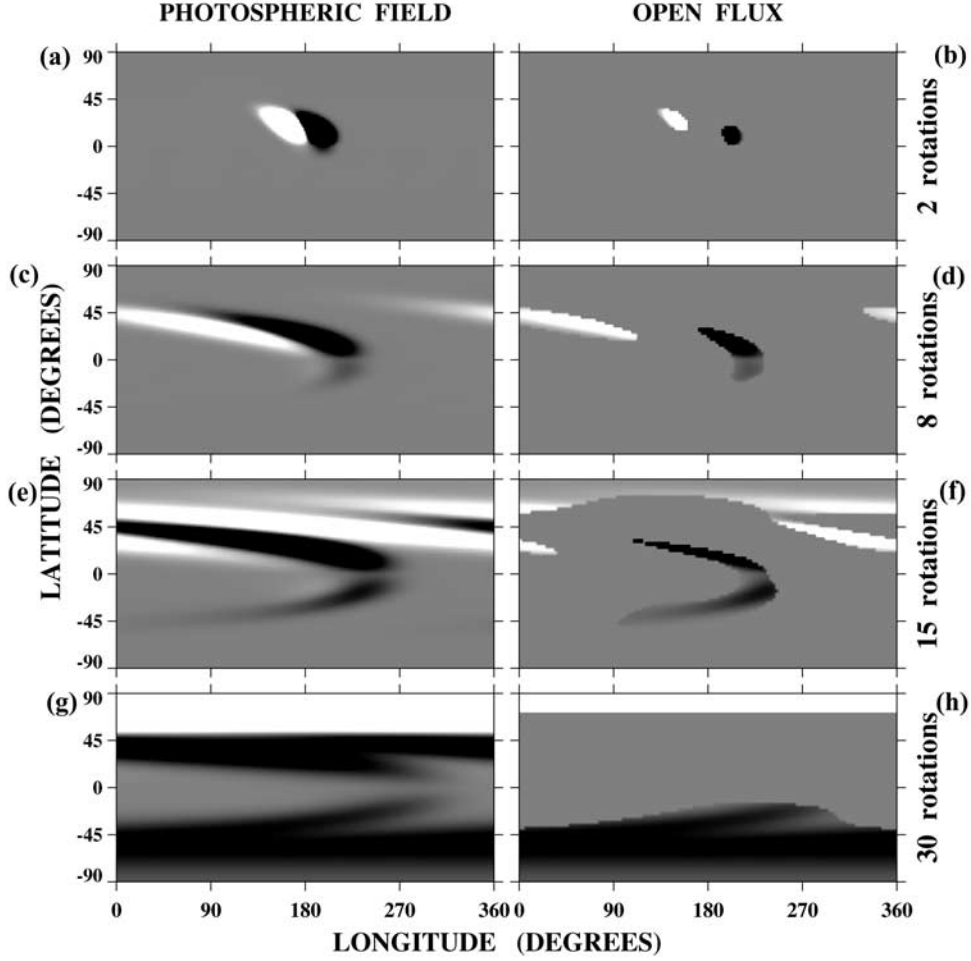


Figure 8. (a–h) Single, large bipolar magnetic region (BMR) evolving under the influence of differential rotation, diffusion, and poleward flow (reference simulation). The bipole was deposited at latitude $\lambda = +15^\circ$ with a total flux $\Phi_{\text{tot}}(0) = 5 \times 10^{23}$ Mx and a longitudinal (latitudinal) pole separation of 20° (4°). The Carrington format maps display the distribution of the photospheric field (Figures 8a, 8c, 8e, and 8g) and the open flux (Figures 8b, 8d, 8f, and 8h) at four different times. Figures 8a and 8b show $t = 2$ rotations. White (black) denotes $B_r > +20$ G ($B_r < -20$ G). Figures 8c and 8d show $t = 8$ rotations. White (black) denotes $B_r > +20$ G ($B_r < -20$ G). Figures 8e and 8f show $t = 15$ rotations. White (black) denotes $B_r > +3$ G ($B_r < -3$ G). Figures 8g and 8h show $t = 30$ rotations. White (black) denotes $B_r > +0.4$ G ($B_r < -0.4$ G).

[20] The flux transport model describes the evolution of the photospheric field when the sources of newly erupting flux are prescribed [see *Sheeley et al.*, 1985]. In the absence of ongoing flux emergence the radially oriented photospheric field $B_r(R_S, \lambda, \phi, t)$ (where t is the time coordinate) is assumed to obey the transport equation

$$\frac{\partial B_r}{\partial t} = -\omega(\lambda) \frac{\partial B_r}{\partial \phi} + \kappa \nabla_{\perp}^2 B_r - \frac{1}{R_S \cos \lambda} \frac{\partial}{\partial \lambda} [v(\lambda) B_r \cos \lambda]. \quad (19)$$

Here ∇_{\perp}^2 denotes the λ and ϕ components of the Laplacian, $\omega(\lambda) = 13.38 - 2.30 \sin^2 \lambda - 1.62 \sin^4 \lambda$ deg d $^{-1}$ is the synodic angular velocity of the photospheric plasma [Snodgrass, 1983], κ is the diffusion coefficient associated with the nonstationary supergranular convection [Leighton, 1964], and $v(\lambda)$ is the poleward flow velocity [see, e.g.,

Komm et al., 1993]. As in the work of *Wang et al.* [1989b], we shall set $\kappa = 600$ km 2 s $^{-1}$ and $|v(\lambda)| = 10$ m s $^{-1} \cos \lambda \sin^{0.01} |\lambda|$, the latter corresponding to a global flow timescale $\tau_{\text{flow}} \sim R_S / (10 \text{ m s}^{-1}) \sim 2.2$ years.

[21] For a given initial distribution $B_r(R_S, \lambda, \phi, 0)$, we solve equation (19) numerically for the photospheric field at subsequent t . We then extrapolate $B_r(R_S, \lambda, \phi, t)$ to the source surface at $r = R_{SS} = 2.5 R_S$, computing the total open flux Φ_{open} and multipole strengths $\langle b_l \rangle$, $\langle b_{lm} \rangle$ as described previously.

5.1. Evolution of Open Flux From a Single Active Region

[22] It is instructive to consider first the evolution of a single active region or active region complex, which we represent by a large bipolar magnetic region (BMR). As an

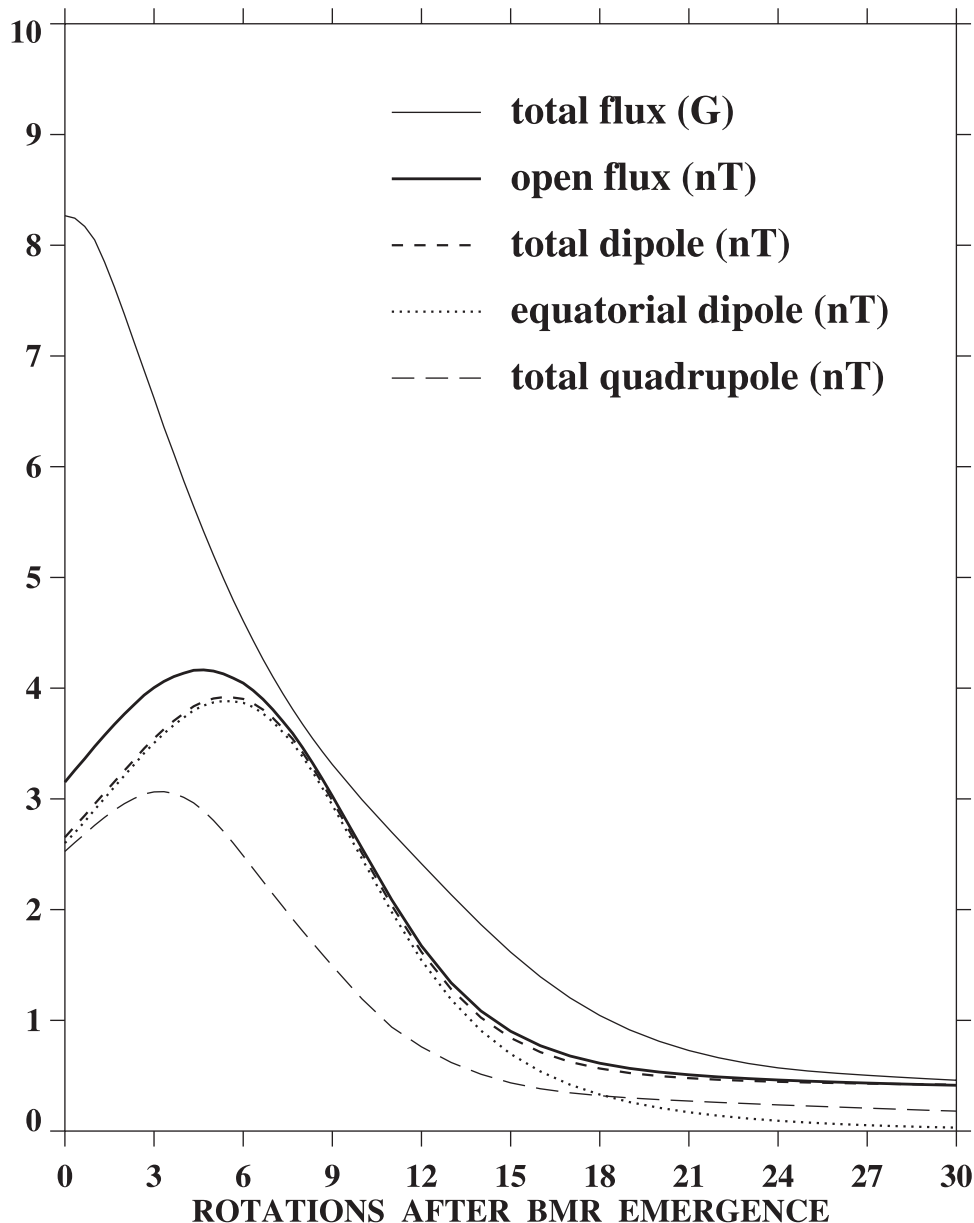


Figure 9. Time evolution of $\Phi_{\text{tot}}/(4\pi R_S^2)$, $\Phi_{\text{open}}/(4\pi r_E^2)$, $\langle b_1 \rangle (R_{ss}/r_E)^2$, $\langle b_{11} \rangle (R_{ss}/r_E)^2$, and $\langle b_2 \rangle (R_{ss}/r_E)^2$ for the reference simulation of Figure 8. The time coordinate is in units of the 27.3-day Carrington period, Φ_{tot} is expressed as a field strength averaged over the solar surface, while Φ_{open} , $\langle b_1 \rangle$, $\langle b_{11} \rangle$, and $\langle b_2 \rangle$ have been converted into equivalent field strengths at $r = r_E = 1$ AU.

illustrative simulation (the “reference case,” also discussed by Wang *et al.* [2000b]), we deposit onto our photospheric grid a magnetic doublet having $\Phi_{\text{tot}}(0) = 5 \times 10^{23}$ Mx, with its negative and positive poles centered at $(\lambda = +13^\circ, \phi = 190^\circ)$ and $(\lambda = +17^\circ, \phi = 170^\circ)$, respectively. (In accordance with “Joy’s law,” the leading or westward pole of the BMR is located equatorward of the trailing pole. This axial tilt, which arises through the action of Coriolis forces on the emerging subsurface toroidal flux, is the source of the axisymmetric field component and thus ultimately of the polar fields [see Wang and Sheeley, 1991; Wang *et al.*, 1989a].) The Carrington format maps in Figure 8 display the distribution of the photospheric field and open flux (coronal holes) after the lapse of 2, 8, 15, and 30 (27.3-day)

rotation periods. At the moment of deposition ($t = 0$) a pair of opposite-polarity coronal holes form at the far corners of the BMR, well away from the polarity inversion line; although small in size, they contain very strong fields, like the holes found near active regions at sunspot maximum. Subsequently, the diffusing BMR flux and the embedded open field regions become increasingly sheared by the photospheric differential rotation. A fraction of the higher-latitude, trailing-polarity flux is gradually carried poleward by the meridional flow, and after $t \sim 15$ rotations a positive-polarity hole begins to form around the North Pole. Meanwhile, a small amount of the lower-latitude, leading-polarity flux diffuses across the equator, giving rise to a negative-polarity hole in the Southern Hemisphere. After 30 rotations

($t = 2.2$ years) all of the open flux is confined to a pair of polar coronal holes, with the one in the Northern Hemisphere being already perfectly axisymmetric.

[23] In Figure 9 we plot the time variation of Φ_{tot} , Φ_{open} , $\langle b_1 \rangle$, $\langle b_{11} \rangle$, and $\langle b_2 \rangle$ during the first 30 rotations. The total BMR flux (which includes closed fields) decreases monotonically as a result of diffusive annihilation at the magnetic neutral line, with the higher- l multipoles decaying first as $\exp[-l(l+1)\kappa t/R_S^2]$. In contrast, the open flux and the dipole strengths initially increase with time, reach a maximum after ~ 5 rotations, and then decline. This behavior can be understood as follows. Since the leading and trailing poles of the BMR are located at different latitudes ($+13^\circ$ and $+17^\circ$, respectively), the photospheric differential rotation moves them apart at a rate $\Delta\omega = 0.09 \text{ deg d}^{-1}$. The equatorial dipole strength $\langle b_{11} \rangle$ is proportional to the longitudinal pole separation and thus initially grows linearly with time, as does $\langle b_1 \rangle \simeq \langle b_{11} \rangle$. Likewise, $d\Phi_{\text{open}}/dt > 0$, since separating the poles of the BMR causes the loops connecting them to expand toward the source surface [Sheeley, 1982]. However, as shearing continues, the rate at which flux is diffusively annihilated (i.e., collapses and submerges below the photosphere) at the ever-lengthening neutral line eventually exceeds the rate at which the outlying flux opens up, and Φ_{open} and $\langle b_{11} \rangle$ begin to decrease.

[24] The winding-up of the photospheric neutral line by differential rotation steepens the latitudinal gradients in $B_r(R_S, \lambda, \phi, t)$ and thus causes the nonaxisymmetric component of the large-scale field to decay more rapidly than it would by diffusion alone [Sheeley *et al.*, 1985]. Meridional flow further accelerates the “stirring” process by carrying flux of both polarities to midlatitudes, where the rotational gradient $|d\omega/d\lambda|$ is largest. By the end of the simulation ($t = 2.2 \text{ years} \sim \tau_{\text{flow}}$), most of the nonaxisymmetric field has been annihilated, leaving the axisymmetric ($m = 0$) dipole component ($\langle b_1 \rangle \rightarrow \langle b_{10} \rangle$), which is unaffected by rotational shearing. As illustrated in Figure 8h, the open flux is now confined to a pair of polar coronal holes, such as might be observed near sunspot minimum.

[25] Although we have ignored the quadrupole component in this discussion, Figure 9 shows that $\langle b_2 \rangle \simeq \langle b_1 \rangle$ during the initial stages of the active region evolution. However, as the BMR spreads and decays, $\langle b_2 \rangle / \langle b_1 \rangle$ decreases steadily, so that after $t \sim 6$ rotations, Φ_{open} is determined almost entirely by the dipole component. This relatively rapid decay of the quadrupole field explains why, in Figure 7a, the $l = 2$ component provides a significant contribution to the open flux only around sunspot maximum, when its strength is maintained through the continual emergence of new active regions.

[26] If the initial configuration $B_r(R_S, \lambda, \phi, 0)$ had included a background polar field, the BMR would have acted either to strengthen or cancel this preexisting field, depending on whether its north-south polarity orientation is the same as or opposite to that of the BMR. The net axisymmetric dipole strength would be obtained simply by summing the values of b_{10} for the BMR and the polar field, resulting in an increase or decrease in the open flux associated with the polar coronal holes. On the other hand, the axisymmetric background field would have no effect on the evolution of the equatorial dipole strength $\langle b_{11} \rangle$. Simulations involving a BMR and a background polar field, in

which quasi-rigidly rotating polar hole extensions are formed, are described by Wang and Sheeley [1990, 1993] and Wang *et al.* [1996].

5.2. Dependence of the Open Flux on the Distribution of Active Regions

[27] While the total magnetic flux of an active region is independent of the field distribution elsewhere on the Sun, the same is not true of its open or closed flux separately. In general, the relative proportions of open and closed flux depend on how the active regions (and the background photospheric field formed from their remnants) are distributed over the solar surface.

[28] To illustrate this point, we now consider the evolution of the open flux from two BMRs, as a function of their relative longitudinal locations. To allow comparison with the previous “reference” simulation, we assign to each BMR a total flux $\Phi_{\text{tot1}}(0) = \Phi_{\text{tot2}}(0) = 2.5 \times 10^{23} \text{ Mx}$, so that the combined value $\Phi_{\text{tot}}(0) = \Phi_{\text{tot1}}(0) + \Phi_{\text{tot2}}(0)$ is the same as that of the single BMR considered above. Each BMR again has a longitudinal (latitudinal) pole separation of 20° (4°). We then compute the evolution of the photospheric and coronal fields for the following four initial configurations (referred to as “cases 1 through 4”): (1) BMRs centered at $(\lambda_1 = +15^\circ, \phi_1 = 135^\circ)$ and $(\lambda_2 = +15^\circ, \phi_2 = 225^\circ)$, both leading poles negative; (2) BMRs centered at $(\lambda_1 = +15^\circ, \phi_1 = 90^\circ)$ and $(\lambda_2 = +15^\circ, \phi_2 = 270^\circ)$, both leading poles negative; (3) BMRs centered at $(\lambda_1 = +15^\circ, \phi_1 = 180^\circ)$ and $(\lambda_2 = -15^\circ, \phi_2 = 180^\circ)$, leading pole negative in the north and positive in the south; and (4) BMRs centered at $(\lambda_1 = +15^\circ, \phi_1 = 90^\circ)$ and $(\lambda_2 = -15^\circ, \phi_2 = 270^\circ)$, leading pole negative in the north and positive in the south. (The reversal of the east-west polarity orientation across the equator is consistent with Hale’s hemispheric rule.) The configurations all have the same axisymmetric dipole strength $\langle b_{10} \rangle$ as in the reference case above, as well as the same initial Φ_{tot} .

[29] Figure 10 displays, for each BMR configuration, the distribution of the photospheric field and open flux after $t = 2$ rotations. In Figure 11, again for each case, we plot Φ_{tot} , Φ_{open} , $\langle b_1 \rangle$, $\langle b_{11} \rangle$, and $\langle b_2 \rangle$ as functions of time. In interpreting the results it will be useful to keep in mind that $b_{11} \propto \pm \sin(\phi - \phi_0)$ and $b_{22} \propto \pm \sin[2(\phi - \phi_0)]$ for a single BMR centered at longitude ϕ_0 , where the sign is determined by its east-west polarity orientation (and we neglect the small correction arising from the axial tilt of the BMR).

[30] In case 1 (two identical BMRs separated by 90° in longitude) the equatorial dipole vectors of the BMRs are perpendicular to each other, so that the resultant value of $\langle b_{11} \rangle$ is reduced by a factor of $\sqrt{2}$ compared to the reference case (Figure 9). Moreover, the (2, 2) quadrupole components of the BMRs are exactly out of phase, so that only the (2, 0) and (2, 1) harmonics contribute to $\langle b_2 \rangle$. The net result is that $\Phi_{\text{open}}(0)$ is about two-thirds as large as in the reference case. In case 2 (two identical BMRs separated by 180° in longitude) the two equatorial dipole vectors are antiparallel to each other, and $\langle b_{11} \rangle = 0$. On the other hand, the (2, 2) components are now in phase again, so that the total quadrupole strength is about the same as in the reference case. The net result is that $\Phi_{\text{open}}(0)$ is reduced by only $\sim 20\%$. However, because it is dominated by the

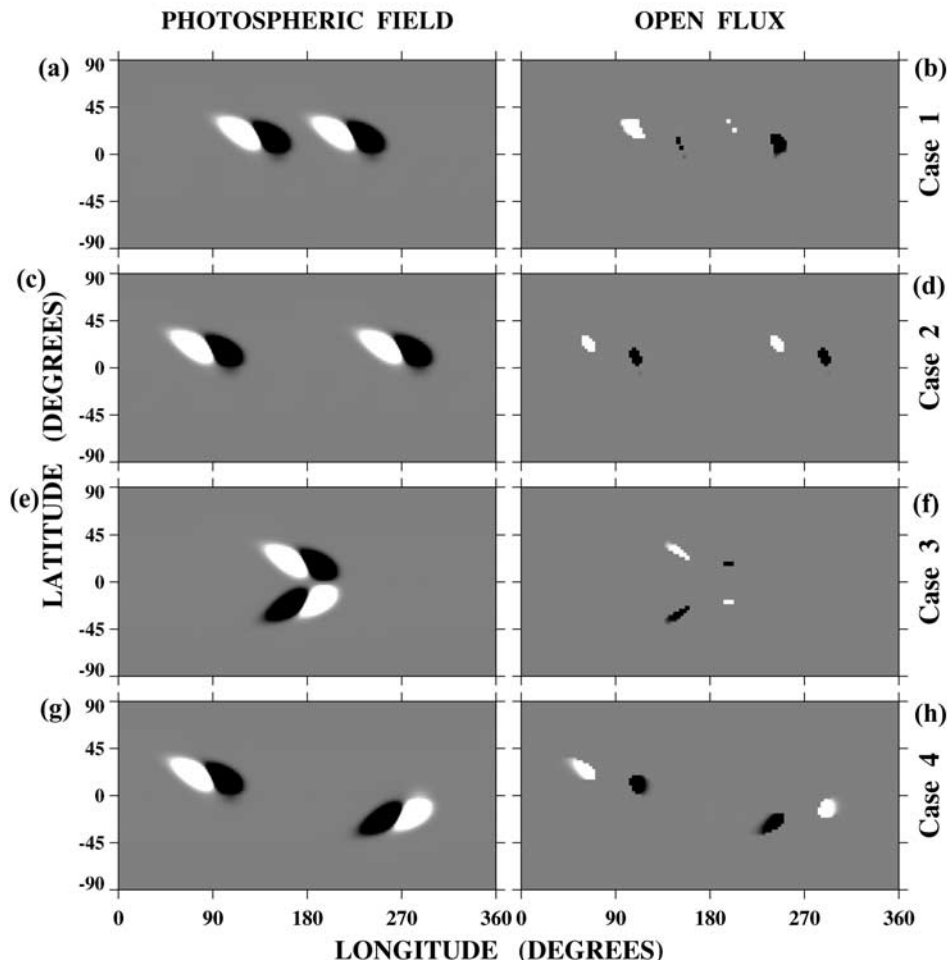


Figure 10. (a–h) Four illustrative simulations involving a pair of BMRs. The Carrington format maps display the distribution of the photospheric field (Figures 10a, 10c, 10e, and 10g) and open flux (Figures 10b, 10d, 10f, and 10h) after $t = 2$ rotations. Each BMR has an initial flux of 2.5×10^{23} Mx and a longitudinal (latitudinal) pole separation of 20° (4°). Case 1 (Figures 10a and 10b) shows BMRs deposited at $\lambda = +15^\circ$ with a longitudinal separation of 90° . Case 2 (Figures 10c and 10d) shows BMRs deposited at $\lambda = +15^\circ$ with a longitudinal separation of 180° . Case 3 (Figures 10e and 10f) shows BMRs deposited at $\lambda = \pm 15^\circ$ with a longitudinal separation of 0° and opposite east-west polarity orientations. Case 4 (Figures 10g and 10h) shows BMRs deposited at $\lambda = \pm 15^\circ$ with a longitudinal separation of 180° and opposite east-west polarity orientations. The gray-scale levels in all maps range between $B_r < -20$ G (black) and $B_r > +20$ G (white).

quadrupole component, the open flux decays considerably more rapidly than in the reference simulation (compare Figure 11b with Figure 9).

[31] In case 3 (both BMRs located at the same longitude but having opposite east-west polarity orientations) the two equatorial dipole vectors again cancel each other, while $\langle b_{22} \rangle = 0$ and $\langle b_2 \rangle = \langle b_{21} \rangle$. This configuration yields the least open flux of all, with $\Phi_{\text{open}}(0)$ being more than a factor of 3 smaller than in the reference case. Finally, in case 4 (two BMRs separated by 180° and having opposite east-west polarity orientations) the equatorial dipole vectors are parallel to each other, and $\langle b_{11} \rangle$ has the same value as in the reference case. Even though this configuration has no $l = 2$ component, the evolution of the total open flux is almost identical to that in the reference simulation (com-

pare Figure 11d with Figure 9), with the absence of the quadrupole being compensated for by the octupole ($l = 3$) component.

[32] It should be noted that the asymptotic behavior of Φ_{open} is approximately the same in all four cases, since it is determined mainly by $\langle b_{10}(0) \rangle$. The final configuration consists of a pair of polar coronal holes extending down to a latitude $|\lambda| \sim 60^\circ$.

[33] The simulations can easily be extended to cases involving multiple sources [see *Sheeley et al.*, 1985; *Wang et al.*, 1989a; *Wang and Sheeley*, 1991]. It is evident that the net dipole strength $\langle b_1(0) \rangle$ is obtained by summing the dipole vectors of the individual BMRs and that the magnitude of $\Phi_{\text{open}}(0)$ is determined by $\langle b_1(0) \rangle$ or $\langle b_1(0) + b_2(0) \rangle$, not by $\Phi_{\text{tot}}(0)$. Again, the annihilation of the equatorial

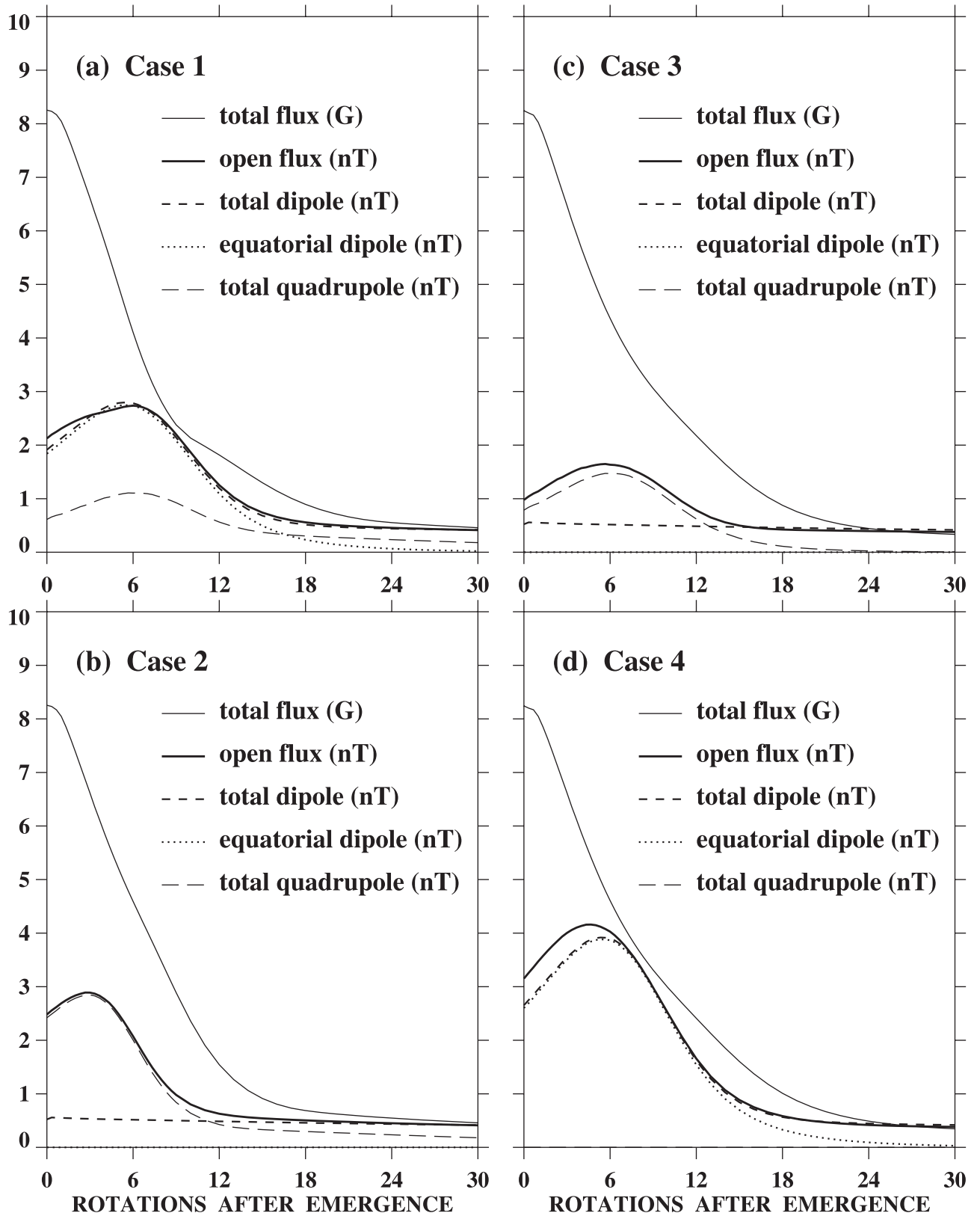


Figure 11. (a–d) Time evolution of $\Phi_{\text{tot}}/(4\pi R_S^2)$, $\Phi_{\text{open}}/(4\pi r_E^2)$, $\langle b_1 \rangle (R_{ss}/r_E)^2$, $\langle b_{11} \rangle (R_{ss}/r_E)^2$, and $\langle b_2 \rangle (R_{ss}/r_E)^2$ for cases 1–4 (see Figure 10).

dipole component on the meridional flow timescale leaves a residual open flux $\Phi_{\text{open}} \propto \langle b_{10}(0) \rangle$.

6. Conclusions

[34] Our conclusions may be summarized as follows:

1. The variation of the radial IMF strength is similar to that of the Sun's total open flux Φ_{open} , as derived from source surface extrapolations of photospheric field measurements, after correction for magnetograph saturation effects. The magnitude of the near-Earth $|B_{\chi}|$ agrees with that obtained on the assumption that Φ_{open} becomes uniformly distributed in solid angle far from the Sun.

2. The average value of Φ_{open} was $\sim 20\%$ – 30% higher during solar cycles 21 and 22 than during cycles 20 and 23, with major peaks occurring in 1982 and 1991.

3. The variation of Φ_{open} approximately follows that of the Sun's total dipole strength, except for a contribution from the magnetic quadrupole ($l = 2$) around sunspot maximum.

4. Both Φ_{open} and the IMF strength show characteristic fluctuations on timescales of ~ 1 year, which correspond to enhancements and subsequent decay of the Sun's nonaxisymmetric dipole component. The enhancements in the equatorial dipole strength are, in turn, a consequence of the episodic, spatially nonuniform nature of large-scale sunspot activity (which is often distributed asymmetrically between the northern and southern or eastern and western hemispheres).

5. The total open flux Φ_{open} shows much less solar cycle modulation than the total photospheric flux Φ_{tot} , which includes closed fields and is dominated by higher-order magnetic multipoles.

6. Near sunspot minimum the open flux originates mainly from the large polar coronal holes; at sunspot maximum it is rooted in small, strong-field regions in the activity zones. The decrease in the total area occupied by coronal holes is offset by the increase in their average field strengths, with the result that Φ_{open} remains roughly the same at sunspot minimum and maximum.

7. Emerging active regions act as sources of new open flux. A given bipolar magnetic region may produce either an increase or a decrease in the Sun's total open flux, depending largely on whether its magnetic dipole vector is oriented so as to reinforce or reduce that of the original photospheric field. In contrast, the emergence of a BMR always causes Φ_{tot} to increase.

8. In the absence of new activity the Sun's equatorial dipole strength and the nonaxisymmetric component of its open flux decay on a timescale ~ 1 year, as meridional flow carries the remnant active region flux to higher latitudes, where the nonaxisymmetric field component is efficiently annihilated by the combined effect of differential rotation and supergranular diffusion. The closed flux suffers a similar fate but also undergoes a rapid initial decline as high-order multipoles decay more or less in place.

9. The Sun's axisymmetric dipole strength, which represents the cumulative sum of the north-south dipole moments of the individual active regions, grows progressively during the declining phase of the cycle (after the reversal of the polar fields).

10. In the asymptotic state (i.e., at sunspot minimum) only the axisymmetric component of the large-scale field survives, in the form of highly concentrated polar fields and polar holes extending down to a latitude of 60° . As long as the poleward surface flow is present and no new activity occurs, neither Φ_{open} nor Φ_{tot} undergoes any further decay.

[35] The main point made in this study is that the Sun's open flux and the IMF strength are determined by the long-lived, lowest-order multipoles of the photospheric field, whereas the total flux is determined mainly by the short-lived, higher-order multipoles, which must be continually regenerated and so are more closely correlated with sunspot activity. However, even in the case of the lowest-order multipoles, the nonaxisymmetric ($m \neq 0$) harmonic components and their associated open flux decay on timescales of ~ 1 year or less and thus also reflect large-scale sunspot activity. It is essentially because of the survival and dominance of the axisymmetric ($m = 0$) dipole component around sunspot minimum that Φ_{open} shows much less solar cycle variation than Φ_{tot} .

[36] In closing, we comment on the assertion by *Lockwood et al.* [1999], based on the striking empirical correlation between the geomagnetic aa index and the radial IMF strength, that the Sun's open flux has undergone a secular increase over the last century. We have found that the average values of Φ_{open} were higher during cycles 21 and 22 than during cycles 20 and 23 (see Figure 1), mainly because the greater rates of flux emergence during the more active sunspot cycles produced larger values of $\langle b_{11} \rangle$, the nonaxisymmetric dipole strength (see Figure 7b). Given the overall increase in sunspot activity since 1900, this result tends to support the claim of Lockwood et al., provided Φ_{open} is averaged over each 11-year cycle or evaluated around sunspot maximum. On the other hand, the secular trend of Φ_{open} between activity minima is less clear, since it depends on the initial polar fields and on the cumulative effect of the very long lived, lowest-order axisymmetric harmonic components.

[37] **Acknowledgments.** We are indebted to J. G. Luhmann and C. "Nick" Arge for motivating us to write this paper and to J. T. Hoeksema (WSO/Stanford) and R. K. Ulrich (MWO/UCLA) for providing the magnetograph data. This work was supported by NASA and by the Office of Naval Research under the "Solar Magnetism and the Earth's Environment" Accelerated Research Initiative.

[38] Janet G. Luhmann thanks Karen Harvey and another referee for their assistance in evaluating this paper.

References

- Balogh, A., et al., The heliospheric magnetic field over the south polar region of the Sun, *Science*, *268*, 1007, 1995.
- Cane, H. V., G. Wibberenz, I. G. Richardson, and T. T. von Roseninge, Cosmic ray modulation and the solar magnetic field, *Geophys. Res. Lett.*, *26*, 565, 1999.
- Cliver, E. W., and A. G. Ling, Coronal mass ejections, open magnetic flux, and cosmic-ray modulation, *Astrophys. J.*, *556*, 432, 2001.
- Gaizauskas, V., K. L. Harvey, J. W. Harvey, and C. Zwaan, Large-scale patterns formed by solar active regions during the ascending phase of cycle 21, *Astrophys. J.*, *265*, 1056, 1983.
- Harvey, K. L., N. R. Sheeley Jr., and J. W. Harvey, Magnetic measurements of coronal holes during 1975–1980, *Sol. Phys.*, *79*, 149, 1982.
- Hoeksema, J. T., J. M. Wilcox, and P. H. Scherrer, Structure of the heliospheric current sheet in the early portion of sunspot cycle 21, *J. Geophys. Res.*, *87*, 10,331, 1982.
- Howard, R., and B. J. LaBonte, Surface magnetic fields during the solar activity cycle, *Sol. Phys.*, *74*, 131, 1981.

- Komm, R. W., R. F. Howard, and J. W. Harvey, Meridional flow of small photospheric magnetic features, *Sol. Phys.*, 147, 207, 1993.
- Leighton, R. B., Transport of magnetic fields on the Sun, *Astrophys. J.*, 140, 1547, 1964.
- Lockwood, M., and R. Stamper, Long-term drift of the coronal source magnetic flux and the total solar irradiance, *Geophys. Res. Lett.*, 26, 2461, 1999.
- Lockwood, M., R. Stamper, and M. N. Wild, A doubling of the Sun's coronal magnetic field during the past 100 years, *Nature*, 399, 437, 1999.
- Mikic, Z., and J. A. Linker, The large-scale structure of the solar corona and inner heliosphere, in *Solar Wind Eight*, edited by D. Winterhalter et al., *AIP Proc.*, 382, 104, 1996.
- Neugebauer, M., et al., Spatial structure of the solar wind and comparisons with solar data and models, *J. Geophys. Res.*, 103, 14,587, 1998.
- Schatten, K. H., Current sheet magnetic model for the solar corona, *Cosmic Electrodyn.*, 2, 232, 1971.
- Schatten, K. H., J. M. Wilcox, and N. F. Ness, A model of interplanetary and coronal magnetic fields, *Sol. Phys.*, 6, 442, 1969.
- Sheeley, N. R., Jr., The coronal field lines of an evolving bipolar magnetic region, *Astrophys. J.*, 255, 316, 1982.
- Sheeley, N. R., Jr., C. R. DeVore, and J. P. Boris, Simulations of the mean solar magnetic field during sunspot cycle 21, *Sol. Phys.*, 98, 219, 1985.
- Smith, E. J., A. Balogh, R. J. Forsyth, and D. J. McComas, Ulysses in the south polar cap at solar maximum: Heliospheric magnetic field, *Geophys. Res. Lett.*, 28, 4159, 2001.
- Snodgrass, H. B., Magnetic rotation of the solar photosphere, *Astrophys. J.*, 270, 288, 1983.
- Suess, S. T., A. K. Richter, C. R. Winge, and S. F. Nerney, Solar polar coronal hole: A mathematical simulation, *Astrophys. J.*, 217, 296, 1977.
- Svalgaard, L., and J. M. Wilcox, Long term evolution of solar sector structure, *Sol. Phys.*, 41, 461, 1975.
- Ulrich, R. K., Analysis of magnetic fluxtubes on the solar surface from observations at Mt. Wilson of $\lambda 5250$ and $\lambda 5233$, in *Cool Stars, Stellar Systems, and the Sun*, edited by M. S. Giampapa and J. A. Bookbinder, p. 265, Astron. Soc. of the Pac., San Francisco, Calif., 1992.
- Ulrich, R. K., S. Evans, J. E. Boyden, and L. Webster, Mt. Wilson synoptic magnetic fields: Improved instrumentation, calibration and analysis applied to the 14 July 2000 flare and to the evolution of the dipole field, *Astrophys. J. Suppl.*, in press, 2002.
- Wang, A. H., S. T. Wu, S. T. Suess, and G. Poletto, Global model of the corona with heat and momentum addition, *J. Geophys. Res.*, 103, 1913, 1998.
- Wang, Y.-M., and N. R. Sheeley Jr., Magnetic flux transport and the sunspot-cycle evolution of coronal holes and their wind streams, *Astrophys. J.*, 365, 372, 1990.
- Wang, Y.-M., and N. R. Sheeley Jr., Magnetic flux transport and the Sun's dipole moment: New twists to the Babcock-Leighton model, *Astrophys. J.*, 375, 761, 1991.
- Wang, Y.-M., and N. R. Sheeley Jr., On potential field models of the solar corona, *Astrophys. J.*, 392, 310, 1992.
- Wang, Y.-M., and N. R. Sheeley Jr., Understanding the rotation of coronal holes, *Astrophys. J.*, 414, 916, 1993.
- Wang, Y.-M., and N. R. Sheeley Jr., Solar implications of Ulysses interplanetary field measurements, *Astrophys. J.*, 447, L143, 1995.
- Wang, Y.-M., A. G. Nash, and N. R. Sheeley Jr., Evolution of the Sun's polar fields during sunspot cycle 21: Poleward surges and long-term behavior, *Astrophys. J.*, 347, 529, 1989a.
- Wang, Y.-M., A. G. Nash, and N. R. Sheeley Jr., Magnetic flux transport on the Sun, *Science*, 245, 712, 1989b.
- Wang, Y.-M., S. H. Hawley, and N. R. Sheeley Jr., The magnetic nature of coronal holes, *Science*, 271, 464, 1996.
- Wang, Y.-M., J. Lean, and N. R. Sheeley Jr., The long-term variation of the Sun's open magnetic flux, *Geophys. Res. Lett.*, 27, 505, 2000a.
- Wang, Y.-M., N. R. Sheeley Jr., and J. Lean, Understanding the evolution of the Sun's open magnetic flux, *Geophys. Res. Lett.*, 27, 621, 2000b.
- White, O. R., and D. E. Trotter, Note on the distribution of sunspots between the north and south solar hemispheres and its variation with the solar cycle, *Astrophys. J. Suppl.*, 33, 391, 1977.
- Wolfson, R., A coronal magnetic field model with volume and sheet currents, *Astrophys. J.*, 288, 769, 1985.
- Zhao, X., and J. T. Hoeksema, A coronal magnetic field model with horizontal volume and sheet currents, *Sol. Phys.*, 151, 91, 1994.
- Zwaan, C., Elements and patterns in the solar magnetic field, *Annu. Rev. Astron. Astrophys.*, 25, 83, 1987.

N. R. Sheeley Jr. and Y.-M. Wang, E. O. Hulburt Center for Space Research, Naval Research Laboratory, Washington, D.C. 20375-5352, USA. (sheeley@spruce.nrl.navy.mil; ywang@yucca.nrl.navy.mil)